

Spin polarized STM spectra of Dirac Fermions on the surface of a topological insulator

K. Saha⁽¹⁾, Sourin Das⁽²⁾, K. Sengupta⁽¹⁾ and D. Sen⁽³⁾

⁽¹⁾ *Theoretical Physics Department, Indian Association for the Cultivation of Science, Jadavpur, Kolkata 700 032, India*

⁽²⁾ *Department of Physics and Astrophysics, University of Delhi, Delhi 110 007, India*

⁽³⁾ *Center for High Energy Physics, Indian Institute of Science, Bangalore 560 012, India*

(Dated: February 17, 2022)

We provide a theory for the tunneling conductance $G(V)$ of Dirac Fermions on the surface of a topological insulator as measured by a spin-polarized scanning tunneling microscope tip for low bias voltages V . We show that $G(V)$ exhibits an unconventional dependence on the direction of magnetization of the tip and can be used to measure the magnitude of the local out-of-plane spin orientation of the Dirac Fermions on the surface. We also demonstrate that if the in-plane rotational symmetry on the surface of the topological insulator is broken by an external field, then $G(V)$ acquires a dependence on the azimuthal angle of the magnetization of the tip. We explain the role of the Dirac Fermions in this unconventional behavior and suggest experiments to test our theory.

PACS numbers: 71.10.Pm, 73.20.-r, 72.25.-b

I. INTRODUCTION

Topological insulators in both two and three dimensions (2D and 3D) have attracted a lot theoretical and experimental attention in recent years¹⁻⁷. It has been shown in Refs. 4–6 that such 3D insulators can be completely characterized by four integers ν_0 and $\nu_{1,2,3}$. The former specifies the class of topological insulators to be strong ($\nu_0 = 1$) or weak ($\nu_0 = 0$) while the latter integers characterize the time-reversal invariant momenta of the system given by $\vec{M} = (\nu_1\vec{b}_1, \nu_2\vec{b}_2, \nu_3\vec{b}_3)/2$, where $\vec{b}_{1,2,3}$ are the reciprocal lattice vectors. The latter integers $\nu_{1,2,3}$ are basis dependent while the former, ν_0 , is a basis-independent invariant for a given material. The weak topological insulators (WTI) are adiabatically connected to Anderson insulators whereas the strong topological insulators (STI) are not; consequently the topological features of STI are robust against the presence of time-reversal invariant perturbations such as disorder or lattice imperfections. STI exhibit a host of novel phenomenon such as induction of magnetic monopoles in the presence of an electric charge near its surface⁸, presence of topologically protected Fermion modes inside dislocations⁹, and the possibility of realization of magnetic control over electrical conduction in its junction¹⁰. It has been theoretically predicted^{1,4} and later experimentally verified² that the surface of a STI has an odd number of Dirac cones whose positions are determined by projection of \vec{M} to the surface Brillouin zone. The position and number of these cones depend on both the nature of the surface concerned and the integers $\nu_{1,2,3}$. For several compounds specific surfaces can be found which will host a single Dirac cone near the Γ point of the 2D Brillouin zone^{2,11}. Such a Dirac cone at the surface of a topological insulator is described by the Dirac Hamiltonian¹²

$$H_0 = \int \frac{d^2k}{(2\pi)^2} \psi^\dagger(\vec{k}) \left[\hbar v_F (\vec{\sigma} \times \vec{k}) \cdot \hat{z} - \mu I \right] \psi(\vec{k}), \quad (1)$$

where $\vec{\sigma}(I)$ denote the Pauli (identity) matrices in spin space, $\psi(\vec{k}) = (\psi_\uparrow(\vec{k}), \psi_\downarrow(\vec{k}))^T$ is the electron annihilation operator, $\vec{k} = (k_x, k_y)$ is the 2D wave vector, \hat{z} denote the unit vector normal to the topological insulator surface, and μ is the chemical potential. The properties of these surface Dirac electrons has been studied in detail in recent years. In particular, these Fermions are expected to exhibit spin-momentum locking which predicts their spin to be along the surface. This phenomenon has been extensively studied by recent spin-resolved ARPES studies^{11,13}. However, in many cases, such studies lead to a finite, albeit small, probability of the measured spin polarization to point along the \hat{z} direction¹⁴. It is unclear at the moment whether this contribution comes due to possible additional higher order terms in the Dirac Hamiltonian of the surface electrons¹⁵ which can spoil the spin-momentum locking property, or due to the presence of additional scattering potentials induced by point-like or step-like defects. Such spin-momentum locking for the surface electrons has also been studied indirectly through scanning tunneling microscope (STM) studies near step edges¹⁶. However, the surface of these insulators has not been studied using spin-polarized STM¹⁷.

In this work we develop a theory for the tunneling current of the Dirac Fermions on the surface of a topological insulator as measured by a spin-polarized STM tip. We derive explicit expressions for the tunneling current $I(V)$ and the tunneling conductance $G(V) = dI(V)/dV$ and show that these quantities exhibit an unconventional dependence on the direction of the tip magnetization. Such an unconventional nature of the tunneling current and conductance originates from the fact that Fermions on the surfaces of topological insulators, in contrast to conventional electrons obeying the Schrödinger equation, exhibit spin-momentum locking which does not allow a free choice of their spin quantization axis (which is fixed along the \hat{z} direction as evident from Eq. (1)). We demonstrate that the analysis of $G(V)$ provides a direct method of measurement of the local out-of-plane spin component

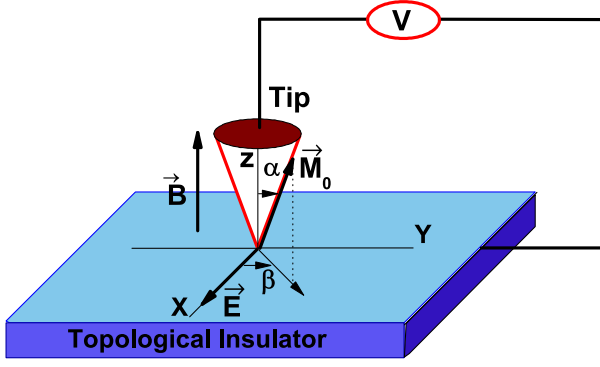


FIG. 1: (Color online) Schematic representation of the proposed experimental setup. The polar (α) and the azimuthal (β) angles of the tip magnetization \vec{M}_0 are shown. The applied electric and magnetic field are along \hat{z} and \hat{x} respectively.

of the Dirac Fermions on the surface. Further, we show that if the in-plane rotational symmetry on the surface of the topological insulator is broken by an external field, then $G(V)$ acquires a dependence on the azimuthal angle of the tip magnetization. We substantiate our theory and demonstrate these unconventional features by a computation of $G(V)$ for Dirac Fermions in the presence of a crossed electric (in-plane along \hat{x}) and magnetic field (out of plane along \hat{z}) as shown in Fig. (1). We suggest experiments which can test our theory.

The organization of the rest of the paper is as follows. In Sec. II, we obtain the general expressions for $I(V)$ and $G(V)$ as measured by a spin-polarized STM tip at low bias voltages V . This is followed by Sec. III where we provide an explicit calculation of the tunneling conductance $G(V)$ for Dirac Fermions on the surface of a topological insulator in the presence of a crossed in-plane electric and out-of-plane magnetic field. We discuss possible experiments and conclude in Sec. IV.

II. TUNNELING CURRENT DUE TO A SPIN-POLARIZED STM

The experimental situation that we intend to describe is schematically shown in Fig. (1). The STM tip is placed atop the surface of the topological insulator and has a magnetization \vec{M}_0 as shown in Fig. (1). To understand the unconventional behavior of the tunneling current in such a system, let us briefly review the current obtained by such a spin-polarized tip when placed atop the surface of a conventional magnetic material with a magnetization $\vec{m}_0(\mathbf{r})$. In this case, the STM current is given by the well known expression^{18,19}

$$I(V) = \frac{2\pi e}{\hbar} \sum_{\mu\nu} \delta(E_\mu^t - E_\nu^s - eV) [f(E_\mu^t) - f(E_\nu^s)] \times |M_{\mu\nu}|^2, \quad (2)$$

where f is the Fermi distribution function, E_μ^t and E_ν^s denote the energy levels of the tip and the surface states respectively, and $M_{\mu\nu}$ denotes the matrix element for overlap between the tip and the STM wave functions which is determined by the Bardeen tunneling formula²⁰

$$M_{\mu\nu} = \frac{\hbar^2}{2m} \int_s ds [\psi_\mu^{t*}(\mathbf{r}, z) \partial_z \psi_\nu^s(\mathbf{r}, z) - \psi_\nu^s(\mathbf{r}, z) \partial_z \psi_\mu^{t*}(\mathbf{r}, z)], \quad (3)$$

where \mathbf{r} denotes only the (x, y) coordinates. Here ψ_μ^t and ψ_ν^s denote the wave functions of the electrons in the tip and on the sample surface respectively, z is taken to be the direction perpendicular to the surface, and the integral is to be performed over a plane which lies between the STM tip and the sample surface and is parallel to the sample surface.

For a conventional magnetic sample, one can always choose the local spin quantization axis to be along the direction of magnetization of the tip. Consequently the wave function of the tip electrons can be written as

$$\psi_\mu^t(\mathbf{r}; z) = (1, 0) \chi_\mu(\mathbf{r}; z), \quad (4)$$

where the precise form of $\chi_\mu(\mathbf{r})$ is difficult to obtain theoretically and it is usually modeled to have the same orbital symmetry of the electron for the atom at the STM tip. For the rest of this work, we shall assume an s -wave symmetric wave function for the tip electrons; all the results obtained can be extended to other orbital symmetries in a straightforward manner using the methods of Ref. 19. Note that such a choice of the spin quantization axis of the tip is possible since both the surface and the tip electrons obey Schrödinger equations which, in contrast to the Dirac equation, do not specify a choice of the spin quantization axis. For the surface electrons, the wave function can be written as

$$\psi_\nu^s(\mathbf{r}, z) = (\cos(\theta_\nu(\mathbf{r})/2), \sin(\theta_\nu(\mathbf{r})/2) e^{i\phi_\nu(\mathbf{r})}) \xi_\nu(\mathbf{r}; z) \quad (5)$$

where the angles $\theta_\nu(\mathbf{r}, z)$ and $\phi_\nu(\mathbf{r}, z)$ are polar and azimuthal angles with respect to the tip magnetization, and $\xi_\mu(\mathbf{r})$ denotes the spatial part of the surface electron wave function whose specific form depends on the system^{19,21}. Using Eqs. (3), (4) and (5), a straightforward analysis following Ref. 21 yields

$$M_{\mu\nu} = c_0 \cos(\theta_\nu(\mathbf{r}_t)/2) \xi_\nu(\mathbf{r}_t), \quad (6)$$

where $\mathbf{r}_t \equiv (\mathbf{r}_t, z_t)$ denotes the position of the tip, and the constant c_0 depends on the details of the tip wave function whose expression for a spherically symmetric s -wave tip is given by^{18,20,21}

$$c_0 = \frac{2\pi N \hbar^2}{\kappa m}, \quad (7)$$

where N is the normalization constant, κ is the decay length of the tip wavefunction, and m is the mass of the

tip electrons. Substituting Eqs. (6) in Eq. (2) one obtains a more familiar expression for the current

$$I(V) = I_0 |c_0|^2 \rho_t(\rho_s(eV; \mathbf{r}_t) + m_s(eV; \mathbf{r}_t)), \quad (8)$$

where V is the applied voltage, $I_0 = 2\pi e/\hbar$, ρ_t is the density of states for the tip electron which is assumed to be constant within the range of experimental applied voltages, and the integrated local density of states $\rho_s \equiv \rho_s(eV; \mathbf{r}_t)$ and magnetization $m_s \equiv m_s(eV; \mathbf{r}_t)$ are given by

$$\begin{aligned} \rho_s &= \int d\omega [f(\omega) - f(\omega + eV)] \\ &\quad \times \sum_{\nu} \delta(E_{\nu} - \omega) |\xi_{\nu}(\mathbf{r}_t)|^2 \\ m_s &= \int d\omega [f(\omega) - f(\omega + eV)] \\ &\quad \times \sum_{\nu} \delta(E_{\nu} - \omega) |\xi_{\nu}(\mathbf{r}_t)|^2 \cos(\theta_{\nu}(\mathbf{r}_t)). \end{aligned} \quad (9)$$

Note that if we restrict ourselves to low bias voltages and low temperatures for which the contribution to m_s comes from a narrow range of ν for which the relative angle of magnetization between the sample and the STM tip is approximately a constant, we obtain

$$I(V) = I_0 |c_0|^2 \rho_t \rho_s(eV; \mathbf{r}_t) [1 + \cos(\theta(\mathbf{r}_t))] \quad (10)$$

which is the well-known expression for the current for a magnetic material as measured by a fully polarized STM tip.

The central result of our work, which we now derive, is that Eq. (10) needs to be significantly modified for the calculation of $I(V)$ for a topological insulator. For a topological insulator, the electrons on the surface are described by the Dirac Hamiltonian given by Eq. (1) with some possible additional warping terms, impurity potentials, and/or external electric and magnetic fields. In all such cases, the spin quantization axis of the electrons is fixed to be along \hat{z} . In this situation, for the system of polarized STM tip near the surface, once we choose to describe the Dirac Fermions by Eq. (1) (with possible additional terms), it is no longer possible to fix the spin quantization axis of the system along the magnetization of the STM tip. Thus the tip wave function has to be represented as

$$\begin{aligned} \psi_{\mu}^t(\mathbf{r}; z) &= \left(\cos(\alpha_{\mu}(\mathbf{r}, z)/2), \sin(\alpha_{\mu}(\mathbf{r}, z)/2) e^{i\beta_{\mu}(\mathbf{r}, z)} \right) \\ &\quad \times \chi_{\mu}(\mathbf{r}; z), \end{aligned} \quad (11)$$

where $\alpha_{\mu}(\mathbf{r}, z)$ and $\beta_{\mu}(\mathbf{r}, z)$ denotes the polar (as measured with respect to \hat{z}) and azimuthal angles of the magnetization (as measured with respect to an in-plane rotational symmetry breaking field along \hat{x} which will be specified later) as shown in Fig. (1). Note that in the absence of an in-plane symmetry breaking field, as shown in Fig. (2), the azimuthal angle can be chosen to have any

arbitrary value. The wave function of the Dirac electrons on the surface of a topological insulator in real space can be written as

$$\begin{aligned} \psi_{\nu}^{\text{TI}}(\mathbf{r}; z) &= (\psi_{\uparrow\nu}^{\text{TI}}(\mathbf{r}; z), \psi_{\downarrow\nu}^{\text{TI}}(\mathbf{r}; z)) \\ &= \left(1, \kappa_{\nu}(\mathbf{r}, z) e^{-i\eta_{\nu}(\mathbf{r}, z)} \right) \psi_{\uparrow\nu}^{\text{TI}}(\mathbf{r}; z) \end{aligned} \quad (12)$$

where $\psi_{\uparrow\nu}^{\text{TI}}(\mathbf{r}; z)$ and $\psi_{\downarrow\nu}^{\text{TI}}(\mathbf{r}; z)$ represent the spin-up and spin-down component of the Dirac electrons and we have used $\psi_{\downarrow\nu}^{\text{TI}}(\mathbf{r}; z)/\psi_{\uparrow\nu}^{\text{TI}}(\mathbf{r}; z) = \kappa_{\nu}(\mathbf{r}, z) \exp[-i\eta_{\nu}(\mathbf{r}, z)]$. We will provide explicit expressions for these wave functions for a specific case in the next section.

Substituting Eqs. (11) and (12) in Eq. (3), one then obtain the matrix element $M_{\mu\nu}$ entering the expression of the current $I(V)$ in Eq. (2) to be

$$\begin{aligned} M_{\mu\nu} &= c_0 \psi_{\uparrow\mu}^{\text{TI}}(\mathbf{r}; z) \left[\cos(\alpha_{\mu}(\mathbf{r}, z)/2) + \kappa_{\nu}(\mathbf{r}, z) \right. \\ &\quad \left. \times \sin(\alpha_{\mu}(\mathbf{r}, z)/2) e^{i[\beta_{\mu}(\mathbf{r}, z) - \eta_{\nu}(\mathbf{r}, z)]} \right] \end{aligned} \quad (13)$$

which yields, assuming constant density of states for the tip and energy independence of the tip magnetization angles α and β ,

$$\begin{aligned} I(V) &= I_0 |c_0|^2 \rho_t \left[\rho_d(eV; \mathbf{r}_t) + \rho_z(eV; \mathbf{r}_t) \cos(\alpha) \right. \\ &\quad \left. + \rho_m(eV, \beta; \mathbf{r}_t) \sin(\alpha) \right] \\ \rho_d(eV; \mathbf{r}_t) &= \frac{1}{2} \int d\omega [f(\omega) - f(\omega + eV)] \\ &\quad \times \sum_{\nu} \delta(E_{\nu} - \omega) |\psi_{\uparrow\nu}^{\text{TI}}(\mathbf{r}_t)|^2 [1 + \kappa_{\nu}^2(\mathbf{r}_t)] \\ \rho_z(eV; \mathbf{r}_t) &= \frac{1}{2} \int d\omega [f(\omega) - f(\omega + eV)] \\ &\quad \times \sum_{\nu} \delta(E_{\nu} - \omega) |\psi_{\uparrow\nu}^{\text{TI}}(\mathbf{r}_t)|^2 [1 - \kappa_{\nu}^2(\mathbf{r}_t)] \\ \rho_m(eV, \beta; \mathbf{r}_t) &= \int d\omega [f(\omega) - f(\omega + eV)] \sum_{\nu} \delta(E_{\nu} - \omega) \\ &\quad \times |\psi_{\uparrow\nu}^{\text{TI}}|^2 \kappa_{\nu}(\mathbf{r}_t) \cos[\beta - \eta_{\nu}(\mathbf{r}_t)] \end{aligned} \quad (14)$$

Using Eq. 14, the tunneling conductance $G(V)$ at $T = 0$ can be obtained from Eq. (14) as

$$\begin{aligned} G &= G_0 |c_0|^2 \rho_t \left[\rho'_d(eV; \mathbf{r}_t) + \rho'_z(eV; \mathbf{r}_t) \cos(\alpha) \right. \\ &\quad \left. + \rho'_m(eV, \beta; \mathbf{r}_t) \sin(\alpha) \right] \\ \rho'_d(eV; \mathbf{r}_t) &= \frac{1}{2} \sum_{\nu} \delta(E_{\nu} - eV) |\psi_{\uparrow\nu}^{\text{TI}}(\mathbf{r}_t)|^2 [1 + \kappa_{\nu}^2(\mathbf{r}_t)] \\ \rho'_z(eV; \mathbf{r}_t) &= \frac{1}{2} \sum_{\nu} \delta(E_{\nu} - eV) |\psi_{\uparrow\nu}^{\text{TI}}(\mathbf{r}_t)|^2 [1 - \kappa_{\nu}^2(\mathbf{r}_t)] \\ \rho'_m(eV, \beta; \mathbf{r}_t) &= \sum_{\nu} \delta(E_{\nu} - eV) |\psi_{\uparrow\nu}^{\text{TI}}|^2 \kappa_{\nu}(\mathbf{r}_t) \\ &\quad \times \cos[\beta - \eta_{\nu}(\mathbf{r}_t)], \end{aligned} \quad (15)$$

where $G_0 = 2\pi e^2/\hbar$.

Eqs. (14) and (15) represent the central result of this work. First, we note that the tunneling conductance displays an unconventional dependence on both the polar and azimuthal angles of the tip magnetization. In particular, $G(V)$ may exhibit a dependence on the azimuthal angle β of the magnetization of the tip which never occurs for STM spectra of conventional magnetic samples. Second, we note that we do not expect this unconventional dependence to show up when the tip is placed on top of a pristine topological insulator surface without any defects and/or in the absence of external fields. In this case, since the spins of the Dirac electrons point along the plane due to spin-momentum locking, one expects $\kappa_\nu(\mathbf{r}_t) = 1$ which leads to $\rho_z = 0$. Further, since the sample is completely isotropic, the sum over all the surface states with a given energy E_ν in Eq. (14) will make the current vanish. This can be seen from the fact that such a sum must be independent of the orientation of the \hat{x} and \hat{y} axis on the surface of the TI; therefore shifting $\eta_\nu \rightarrow \eta_\nu + c$ should not change any of the results. Hence, the quantity ρ_m in Eq. (14) must be independent of the choice of β and must therefore vanish. This leads to $I(V) = I_0 |c_0|^2 \rho_t \rho_d (eV; \mathbf{r}_t)$ which is independent of both α and β . Finally, we would like to point out that the presence of a non-zero component of S_z due to warping¹⁵ or other effects such as presence of defects¹⁶ renders $\kappa_\nu(\mathbf{r}_t) \neq 1$ and hence leads to a $\cos(\alpha)$ dependence of $I(V)$ and $G(V)$. Thus measuring $G(V)$ with a spin-polarized STM provides a direct way of measuring the real-space out-of-plane spin polarization of the Dirac electrons on the surface of a topological insulator. We shall discuss this point in more details in Sec. IV.

In the next section, we compute $G(V)$ for the Dirac electrons in the presence of a crossed electric (along \hat{x}) and magnetic field (along \hat{z}) and show that $G(V)$ displays all the unconventional features discussed above.

III. CROSSED ELECTRIC AND MAGNETIC FIELD

In this section, we compute $G(V)$ for the geometry shown in Fig. (1), *i.e.*, in the presence of a constant magnetic field B along \hat{z} and an electric field E along \hat{x} . Throughout this section, we shall assume that the applied magnetic field is weak enough so as not to orient the magnetization of the tip along B . For a stronger magnetic field, one needs to apply the magnetic field along the direction of the magnetization of the tip. Note that for the topological insulator, this just amounts to changing $B \rightarrow B_z = B \cos(\alpha)$ since the in-plane component of the field appears to be a gauge shift for the Dirac electrons and does not have any influence on their properties¹⁰. So all of the analysis of the present section will hold in this case, with $B \rightarrow B \cos(\alpha)$.

We first look for the solution of the wave function $\psi_{\nu\uparrow,\downarrow}^{\text{TI}}(\mathbf{r}, z) = \psi_{\nu\uparrow,\downarrow}^{\text{TI}}(\mathbf{r}) \exp(-\kappa_z z)$, where κ_z is the decay length of the wave function in real space which depends

on the work function of the topological insulator surface. For estimating $G(V)$, we need the value of the wave function at the position of the tip, *i.e.*, at $z = z_t$. Thus it is possible to absorb $\exp(-\kappa_z z_t)$ in the definition of G_0 and one does not need to know the precise value of κ_z to estimate G . The solution for $\psi_{\mu\uparrow,\downarrow}^{\text{TI}}(\mathbf{r})$ and the corresponding energies E_ν for the present configuration is well-known^{10,22}. We will assume that the electric field is smaller than the magnetic field ($E < v_F B$); then one can use a Lorentz transformation to go to a frame where the electric field is zero, solve the Landau level problem in that frame, and then Lorentz transform back to the original frame. The energy eigenstates are labeled by the Landau level index n and the transverse momenta k_y and can be expressed in terms of $\lambda = \text{arccosh}[(1 - E^2/v_F^2 B^2)^{-1/2}]$ for $n \neq 0$ by

$$\begin{aligned} \psi_{n,k_y,\uparrow}^{\text{TI}}(\mathbf{r}) &= [\cosh(\lambda/2)\chi_{n-1}(\xi) + i \sinh(\lambda/2)\chi_n(\xi)] e^{ik_y y}, \\ \psi_{n,k_y,\downarrow}^{\text{TI}}(\mathbf{r}) &= [\cosh(\lambda/2)\chi_n(\xi) - i \sinh(\lambda/2)\chi_{n-1}(\xi)] e^{ik_y y}, \\ E_{n,k_y} &= \text{Sgn}(n)E_0 \cosh(\lambda)^{-3/2} \\ &\quad \times \sqrt{|n| + c_z B \cosh(\lambda)} - \hbar k_y E/B, \end{aligned} \quad (16)$$

where $E_0 = \hbar v_F l_B^{-1}$, $\chi_n = \exp(-\xi^2/2) H_n(\xi)/\sqrt{2^n |n|!}$, H_n denotes Hermite polynomials, $l_B = \sqrt{\hbar c/eB}$ is the magnetic length, $c_z = g^2 \mu_B^2/(\hbar v_F^2 e)$, g is the gyromagnetic ratio, μ_B is the Bohr magneton, and ξ is given by

$$\xi = (x - k_y l_B^2)/\sqrt{\gamma l_B^2 + 2|n|E/(v_F B)}. \quad (17)$$

From Eq. (16), one obtains the parameters κ and η to be

$$\begin{aligned} \kappa_{n,k_y}(x) &= \frac{\sqrt{\cosh^2(\lambda/2)\chi_n^2(\xi) + \sinh^2(\lambda/2)\chi_{n-1}^2(\xi)}}{\sqrt{\cosh^2(\lambda/2)\chi_{n-1}^2(\xi) + \sinh^2(\lambda/2)\chi_n^2(\xi)}}, \\ \eta_{n,k_y}(x) &= \arctan[\tanh(\lambda/2)\chi_n(\xi)/\chi_{n-1}(\xi)] \\ &\quad + \arctan[\tanh(\lambda/2)\chi_{n-1}(\xi)/\chi_n(\xi)]. \end{aligned} \quad (18)$$

The corresponding expressions for the $n = 0$ Landau level are given by

$$\begin{aligned} E_{n,k_y} &= -g\mu_B B/\cosh(\lambda) - \hbar k_y E/B, \\ \psi_{n,k_y,\uparrow}^{\text{TI}}(\mathbf{r}) &= e^{ik_y y} i \sinh(\lambda/2)\chi_0(\xi), \\ \psi_{n,k_y,\downarrow}^{\text{TI}}(\mathbf{r}) &= e^{ik_y y} \cosh(\lambda/2)\chi_0(\xi), \end{aligned} \quad (19)$$

which leads to $\kappa_0 = \coth(\lambda/2)$ and $\eta_0 = -\pi/2$ independent of k_y . We note here that for typical topological insulators $g\mu_B B/E_0 \sim 10^{-4}$ for $B \simeq 1\text{T}$ and so the Zeeman term can be safely neglected in all numerical estimates of G .

To obtain G , we substitute Eqs. (16) and (18) in Eq. (15). In what follows, we choose the STM tip to be directly on top of the origin of coordinates so that $\mathbf{r}_t = (0, 0)$. We note that corresponding to any given applied voltage V , the solution of $E_{n,k_y} = eV$ constitutes, in principle, an infinite number of pairs (n, k_y) . However, the Gaussian factor $\exp(-\xi^2/2)$ in the expression

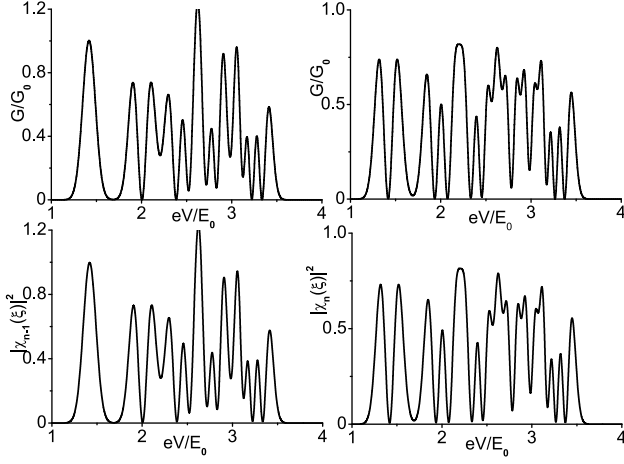


FIG. 2: (Color online) Plot of G/G_0 as a function of the applied voltage eV/E_0 for $\alpha = 0$ (top left panel) and $\alpha = \pi$ (top right panel) for $E/v_F B = 0.1$ and $|c_0|^2 \rho_t/E_0 = 1$. The bottom panels show the variation of the wave functions $|\chi_{n-1}(\xi)|^2$ (bottom left) and $|\chi_n(\xi)|^2$ (bottom right) corresponding to the solution (n, k_y) of $eV = E_n(k_y)$ which contributes maximally to G . See text for details.

of $\psi_{n,k_y,\uparrow}^{\text{TI}}(\mathbf{r})$ and the discrete values of n ensures that out of all these pairs, the one with the minimal value of $|k_y|$ provides the most significant contribution to G . This is particularly valid for small $E \ll v_F B$ which is also the regime we are interested in. In this regime, the tunneling conductance $G(V)$ as a function of V , as computed using Eqs. (16), (19) and (15), is shown in the top left (right) panel of Fig. (2) for $E/v_F B = 0.1$ and $\alpha = 0$ (π). From Eq. (15), we find that for both $\alpha = 0$ and $\alpha = \pi$, $\rho'_m = 0$, so that one has

$$\begin{aligned} G(V; \alpha = 0) &= G_0 |c_0|^2 \rho_t \sum_{\nu} \delta(E_{\nu} - eV) |\psi_{\uparrow\nu}^{\text{TI}}(0)|^2, \\ G(V; \alpha = \pi) &= G_0 |c_0|^2 \rho_t \sum_{\nu} \delta(E_{\nu} - eV) |\psi_{\downarrow\nu}^{\text{TI}}(0)|^2. \end{aligned} \quad (20)$$

The nature of $G(V)$ can now be understood from Eqs. (16) and (19). From these equations, we find that as V is changed so that it deviates from the energy of a Landau level, the lowest value of $k_y \equiv k_y^0$ which is a solution to $eV = E_{n,k_y}$ starts to increase. This leads, through a change of $\xi(k_y^0)$, to a non-monotonic change in the wave functions $|\psi_{\uparrow\nu}^{\text{TI}}(0)|^2$ (for $\alpha = 0$) and $|\psi_{\downarrow\nu}^{\text{TI}}(0)|^2$ (for $\alpha = \pi$) since these wave functions involve a product of the Gaussian factor $\exp(-\xi^2/2)$ and the Hermite polynomials $H_{n-1}(\xi)$ and $H_n(\xi)$. Note that for $E/v_F B = 0.1$, the predominant contribution to $|\psi_{\uparrow\nu}^{\text{TI}}(0)|^2$ [$|\psi_{\downarrow\nu}^{\text{TI}}(0)|^2$] comes from the coefficients of the $\cosh(\lambda/2)$ terms and thus involve $H_{n-1}(\xi)$ [$H_n(\xi)$] for $\alpha = 0$ [π]. In fact, the plots of $\chi_{n-1}[\xi(k_y^0)]$ ($\chi_n[\xi(k_y^0)]$) as a function of V in the lower left(right) panel of Fig. (2) (for $\alpha = 0$ (π)) show that the non-monotonic behavior of $G(V)$ can be understood in terms of the variation of these wave functions with the

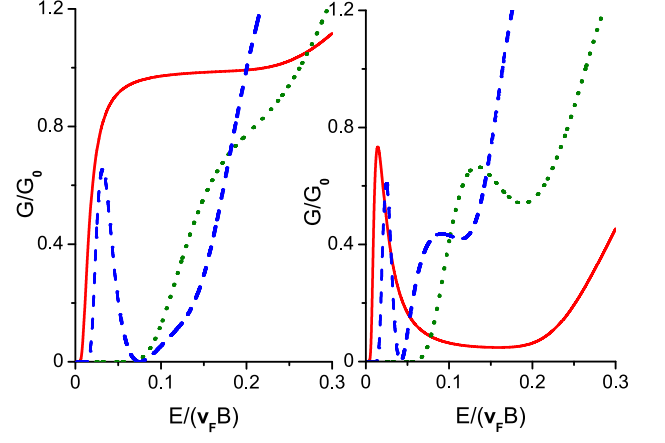


FIG. 3: (Color online) Plot of G/G_0 as a function of the applied electric field $E/v_F B$ for several applied voltages $eV/E_0 = 1.4$ (red solid line), 1.8 (green dotted line), and 2.4 (blue dashed line) for which the maximally contributing (n, k_y) pair corresponds to $n = 1, 2$ and 3 . The left (right) panel corresponds to $\alpha = 0$ (π). We have taken $|c_0|^2 \rho_t/E_0 = 1$ in all the plots. See text for details.

change of k_y^0 as a function of V . We note that the spectral features in $G(V)$ are expected to change drastically with the direction of the tip magnetization as is evident from comparing the left and right panels of Fig. (2).

Next, we fix the applied voltage eV/E_0 and study the behavior of $G(V)$ as a function of the electric field $E/v_F B$ for several values of eV/E_0 for $\alpha = 0$ (left panel) and π (right panel) as shown in Fig. (3). The nature of these plots can again be understood from the variation of the wave functions $\psi_{\uparrow\nu}^{\text{TI}}(0)$ and $\psi_{\downarrow\nu}^{\text{TI}}(0)$. For example, let us consider the plot corresponding to $eV/E_0 = 1.4$ (red solid lines in Fig. (3)) for which the maximally contributing (n, k_y) pair corresponds to $n = 1$. As one increases $E/v_F B$, we find from Eq. (17) that the value of ξ decreases since the decrease in k_y overcompensates for the increase in E leading to a net decrease in ξ in the regime where $E/v_F B \ll 1$. Consequently, for $\alpha = 0$, where G depends on $|\psi_{\uparrow\nu}^{\text{TI}}(0)|^2 \sim |\chi_0(\xi)|^2 \sim \exp(-\xi^2)$, we find an increase in $G(V)$. For $\alpha = \pi$, where G depends on $|\psi_{\downarrow\nu}^{\text{TI}}(0)|^2 \sim |\chi_1(\xi)|^2 \sim \exp(-\xi^2/2) H_1(\xi)^2$, a similar increase in ξ leads to a non-monotonic behavior of G . The plots of G for other values of eV/E_0 shown in Fig. (3) can be understood in a similar manner.

Finally, we consider the variation of the tunneling conductance as a function of the polar (α) and azimuthal (β) angles corresponding to the direction of the tip magnetization for an applied voltage $eV/E_0 = 1.4$ and electric field $E/v_F B = 0.1$ as shown in Fig. (4). We note that $G(V)$ shows maximal variation with β for $\alpha = \pi/2$ as expected from the expression of ρ'_m in Eq. (15). Such a variation is highlighted in Fig. (5) where the plot of G'/G_0 (where $G' = \partial G/\partial \beta$) is shown as a function of β for $\alpha = \pi/2$. We note that since $G'(\beta = 0, \alpha = \pi/2) \sim \sin(\eta(\mathbf{r}_t; V))$, the intercept of this plot is a measure of

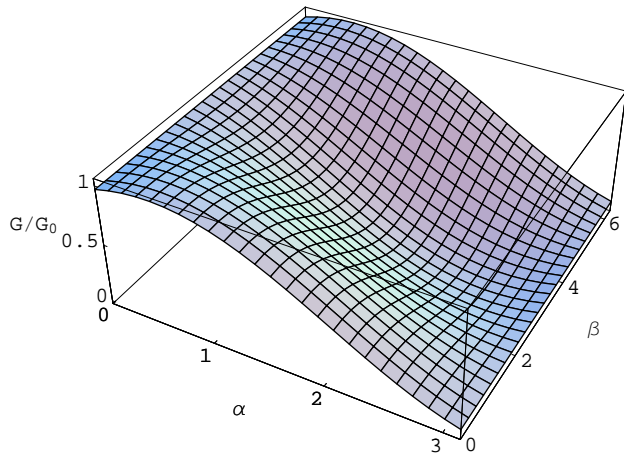


FIG. 4: (Color online) Plot of G/G_0 as a function of the angles α and β for $E/v_F B = 0.1$, $|c_0|^2 \rho_t/E_0 = 1$, and $eV/E_0 = 1.4$.

the local relative phase between the spin-up and spin-down components of the surface Dirac Fermions. Such a variation of the tunneling conductance with the azimuthal angle of the tip magnetization is a novel feature of the topological insulators which originates from fixing the spin quantization axis of the surface Dirac electrons along \hat{z} , and it has no analog in conventional magnets. We note that the measurement of such a variation in an experiment does not require a change in the direction of the tip magnetization. It can simply be achieved by changing the direction of the electric field E which breaks rotational symmetry since β is always defined with respect to the direction of E .

IV. EXPERIMENTS

The experimental test of our work involves measurement of the STM spectra of a topological insulator using a magnetic tip. We note that such measurements can be used to map the spatial out-of-plane spin-orientation profile of the surface Dirac electrons. In particular, we suggest measurement of the spectra with the STM tip magnetization pointing along \hat{z} ($\alpha = 0$) and $-\hat{z}$ ($\alpha = \pi$). The local \hat{z} component of the spin of the Dirac electron can then be obtained from

$$S_z(V) \sim \frac{G(V; \alpha = 0) - G(V; \alpha = \pi)}{G(V; \alpha = 0) + G(V; \alpha = \pi)}. \quad (21)$$

We note that such a measurement would provide direct information about the real-space out-of-plane spin pro-

file of the surface Dirac electrons near surface defects such as point impurities and step edges. The other experiment we suggest involves measurement of the STM spectra with a tip whose magnetization points along the surface of the topological insulator ($\alpha = \pi/2$) in the presence of a crossed electric and magnetic field. Our central

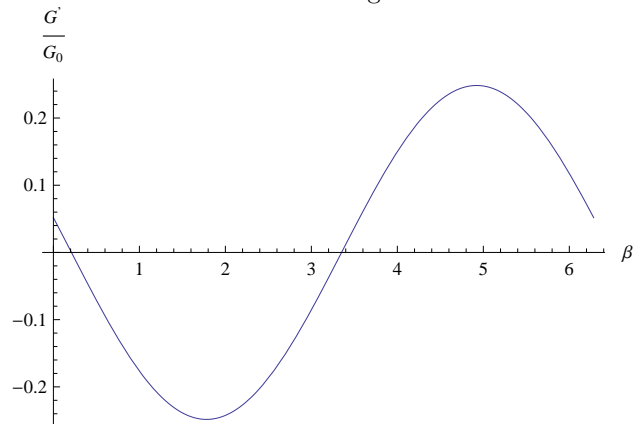


FIG. 5: (Color online) Plot of $G'(V)/G_0$ (where $G' = \partial G/\partial \beta$) as a function of β for $E/v_F B = 0.1$, $|c_0|^2 \rho_t/E_0 = 1$, $\alpha = \pi/2$, and $eV/E_0 = 1.4$.

prediction is that the tunneling conductance will display an oscillatory behavior with the change of the azimuthal angle β (which can be varied by changing the direction of the applied electric field for a fixed tip magnetization) as can be seen from plot of $\partial G/\partial \beta$ as a function of β in Fig. (5). We also note that the value of $G'(\beta = 0)$ provides direct information about the local relative phase of between the spin-up and spin-down components of the electron wavefunction on the topological insulator surface.

In conclusion, we have presented a general theory for the STM spectra of Dirac electrons on the surface of a topological insulator as measured by a magnetic STM tip and have shown that such a spectrum has unconventional features not commonly seen in its counterpart in conventional magnets. We have identified the reason for such an unconventional spectrum to be the fixation of the spin quantization axis of the surface Dirac electrons along the \hat{z} direction. We have also explicitly computed the STM spectra for the surface Dirac electrons in the presence of a crossed electric and magnetic field which demonstrates this unconventional behavior.

KS thanks H. Manoharan, G. Refael, N-C Yeh, and E. Zhao for several related discussions and DST, India for support through grant no. SR/S2/CMP-001/2009. DS thanks DST, India for financial support under SR/S2/JCB-44/2010.

¹ B. A. Bernevig, T. L. Hughes, and S. C. Zhang, *Science* **314**, 1757 (2006).

² D. Hsieh, D. Qian, L. Wray, Y. Xia, Y. S. Hor, R. J. Cava, M. Z. Hasan, *Nature* **452**, 970 (2008).

- ³ C. L. Kane and E. J. Mele, Phys. Rev. Lett. **95**, 226801 (1995); *ibid*, Phys. Rev. Lett. **95**, 146802 (2006).
- ⁴ L. Fu, C. L. Kane, and E. J. Mele, Phys. Rev. Lett. **98**, 106803 (2007).
- ⁵ R. Roy, Phys. Rev. B **79**, 195322 (2009).
- ⁶ J. E. Moore, and L. Balents, Phys. Rev. B **75**, 121306 (2007).
- ⁷ M. König, S. Wiedmann, C. Brüne, A. Roth, H. Buhmann, L. W. Molenkamp, X.-L. Qi, and S.-C. Zhang, Science **318**, 766 (2007).
- ⁸ X. Qi, R. Li, J. Zang, and S. C. Zhang, Science **323**, 1184 (2009).
- ⁹ Y. Ran, Y. Zhang, and A. Vishwanath, Nature Phys. **1220** (2009).
- ¹⁰ S. Mondal, D. Sen, K. Sengupta and R. Shankar, Phys. Rev. Lett. **104**, 046403 (2010); *ibid*, Phys. Rev. B **82**, 045120 (2010).
- ¹¹ Y. Xia, D. Qian, D. Hsieh, L. Wray, A. Pal, H. Lin, A. Bansil, D. Grauer, Y. S. Hor, R. J. Cava, M. Z. Hasan, Nature Phys. **5**, 398 (2009); D. Hsieh, Y. Xia, L. Wray, D. Qian, A. Pal, J. H. Dil, J. Osterwalder, F. Meier, G. Bihlmayer, C. L. Kane, Y. S. Hor, R. J. Cava, and M. Z. Hasan, Science **323**, 919 (2009); D. Hsieh, Y. Xia, D. Qian, L. Wray, J. H. Dil, F. Meier, L. Patthey, J. Osterwalder, A. V. Fedorov, H. Lin, A. Bansil, D. Grauer, Y. S. Hor, R. J. Cava, and M. Z. Hasan, Nature **460**, 1101 (2009); Y. Xia, D. Qian, D. Hsieh, R. Shankar, H. Lin, A. Bansil, A. V. Fedorov, D. Grauer, Y. S. Hor, R. J. Cava, and M. Z. Hasan, arXiv:0907.3089 (unpublished).
- ¹² L. Fu and C. L. Kane, Phys. Rev. Lett. **100**, 096407 (2008).
- ¹³ Su-Yang Xu, L. A. Wray, Y. Xia, R. Shankar, S. Jia, A. Fedorov, J. H. Dil, F. Meier, B. Slomski, J. Osterwalder, R. J. Cava, and M. Z. Hasan, arXiv:1008.3557 (unpublished).
- ¹⁴ Z.-H. Pan, E. Vescovo, A. V. Fedorov, D. Gardner, Y. S. Lee, S. Chu, G. D. Gu, and T. Valla, arXiv:1101.5615 (unpublished).
- ¹⁵ L. Fu, Phys. Rev. Lett. **103**, 266801 (2009).
- ¹⁶ H. Manoharan, private communication.
- ¹⁷ Spin polarized STM measurements have been suggested for possible detection of spin fractionalization in helical Luttinger liquid at the edge of a 2D spin quantum Hall system; see S. Das and S. Rao, arXiv:1006.2239 (unpublished).
- ¹⁸ D. Wortmann, S. Heinze, P. Kurz, G. Bihlmayer, and S. Blugel, Phys. Rev. Lett. **86**, 4132 (2001).
- ¹⁹ C. J. Chen, Phys. Rev. Lett. **65**, 448 (1990); *ibid.*, Phys. Rev. B **42**, 8841 (1990).
- ²⁰ J. Bardeen, Phys. Rev. Lett. **6**, 57 (1961).
- ²¹ J. Tersoff and D. R. Hamann, Phys. Rev. Lett. **50**, 1998 (1983).
- ²² V. Lukose, R. Shankar, and G. Baskaran, Phys. Rev. Lett. **98**, 116802 (2007).